ADVANCED MATERIALS
www.advmat.de

Mechanically Defined Microenvironment Promotes Stabilization of Microvasculature, Which Correlates with the Enrichment of a Novel Piezo-1$^+$ Population of Circulating CD11b$^+$/CD115$^+$ Monocytes

*Aurelien Forget, Roberto Gianni-Barrera, Andrea Uccelli, Melika Sarem, Esther Kohler, Barbara Fogli, Manuele G. Muraro, Sandrine Bichet, Konrad Aumann, Andrea Banfi, and V. Prasad Shastri**

Vascularization is a critical step in the restoration of cellular homeostasis. Several strategies including localized growth factor delivery, endothelial progenitor cells, genetically engineered cells, gene therapy, and prevascularized implants have been explored to promote revascularization. But, long-term stabilization of newly induced vessels remains a challenge. It has been shown that fibroblasts and mesenchymal stem cells can stabilize newly induced vessels. However, whether an injected biomaterial alone can serve as an instructive environment for angiogenesis remains to be elucidated. It is reported here that appropriate vascular branching, and long-term stabilization can be promoted simply by implanting a hydrogel with stiffness matching that of fibrin clot. A unique subpopulation of circulating CD11b$^+$ myeloid and CD11b$^+$/CD115$^+$ monocytes that express the stretch activated cation channel Piezo-1, which is enriched prominently in the clot-like hydrogel, is identified. These findings offer evidence for a mechanobiology paradigm in angiogenesis involving an interplay between mechanosensitive circulating cells and mechanics of tissue microenvironment.

In peripheral artery disease, establishment of new vasculature is critical for rescuing the ischemic tissue and it is a necessary step for successful engraftment of a transplanted tissue/organ. Therapeutic angiogenesis, is a clinical strategy pioneered by Takeshita et al., to induce new blood vessels (collateral vessels) in ischemic tissues from existing vasculature using external cues.[1] The repertoire of external cues range from localized delivery of proangiogenic factors (vascular endothelial growth factor (VEGF),[2] fibroblast growth factor (FGF)[3]), endothelial progenitor cells,[4] cells genetically engineered to secrete a single or a combination of proangiogenic factors,[5] and gene therapy.[6] More recently hypoxia-based strategies including preconditioning of mesenchymal stem cells (MSCs) to hypoxia before transplantation,[7] and gene therapy to locally engineer cells to express hypoxia inducible factor-1α have also been explored. One of the challenges with local delivery of proangiogenic signals, such as VEGF, is that the sprouting and maturation of new vessels into normal or aberrant (tumor-like vessels) depends on the formation of precise concentration gradients in the vessel microenvironment. These depend both on the combination of different isoforms of VEGF with varying affinity for extracellular matrix and their local concentration,[8] which are very difficult to modulate and control. After injury, endothelial cells (ECs) lose their quiescence and get primed and

Dr. A. Forget, Dr. M. Sarem, E. Kohler, Prof. V. P. Shastri
Institute for Macromolecular Chemistry
University of Freiburg
79104 Freiburg, Germany
E-mail: prasad.shastri@gmail.com,
prasad.shastri@makro.uni-freiburg.de
Dr. R. Gianni-Barrera, A. Uccelli, B. Fogli, Dr. M. G. Muraro, Dr. A. Banfi
Department of Biomedicine
University of Basel
Basel 4056, Switzerland
Dr. R. Gianni-Barrera, A. Uccelli, Dr. M. G. Muraro, Dr. A. Banfi
Department of Surgery
University Hospital Basel
Basel 4056, Switzerland
Dr. M. Sarem, Prof. V. P. Shastri
BIOSS Centre for Biological Signaling Studies
University of Freiburg
79104 Freiburg, Germany
Dr. S. Bichet
Friedrich Miescher Institute for Biomedical Research
Basel 4058, Switzerland
Dr. K. Aumann
Institute for Surgical Pathology, Medical Center University of Freiburg
Faculty of Medicine
University of Freiburg
79104 Freiburg, Germany
The ORCID identification number(s) for the author(s) of this article can be found under https://doi.org/10.1002/adma.201808050.

DOI: 10.1002/adma.201808050

become sensitive to external proangiogenic cues. Maintenance of the neovasculature is however vital for vascular homeostasis. In this regard, perivascular cells, i.e., pericytes and vascular smooth muscle cells play a critical role in vivo in not only providing scaffolding but also paracrine signaling necessary for blood vessel sprouting and maturation,[9] In therapeutic angiogenesis, vessels often fail to mature and regress over time[10] due to inadequate recruitment of appropriate support cells, and it has been shown that coculturing of ECs with MSCs[11] or fibroblasts[12] prior to implantation can promote stabilization of new blood vessels and their perfusion. Nonetheless, strategies to promote maturation and stabilization of neovasculature through endogenous mechanisms could be more translatable.

During angiogenesis, ECs express αv family of integrins, which are transmembrane proteins that specifically bind to the arginine–glycine–aspartic acid (RGD) sequence found in many extracellular matrix (ECM) molecules including collagen, fibronectin, and vitronectin.[13] Since integrins are also anchored to the actin cytoskeleton of the cell,[14] they function as mechanotransducers and assist the cells in perceiving the mechanics of the ECM; and it has been shown that integrin signaling is necessary for both EC survival and proliferation.[15] In spite of this compelling evidence linking mechanical cues to EC function, the impact of the ECM mechanical properties on blood vessel sprouting and maturation remains unknown. We had recently demonstrated in vitro that soft carboxylated agarose (CA) hydrogel in combination with RGD-signaling and soluble proangiogenic signals (VEGF, FGF-2, and phorbol-12-myristate 13-acetate (PMA)) can promote the apical-basal polarization of ECs and their organization into freestanding multicellular lumens.[16] Encouraged by this observation, in this study we inquired if the mere introduction of CA hydrogels of appropriate mechanical properties could be sufficient to promote maturation and stabilization of neovasculature in vivo. Specifically, we chose a 2% w/v solution of CA with 28% and 60% carboxylation as they yielded gels of two distinct stiffness (5 kPa (stiff gel) and 0.5 kPa (soft gel), respectively) that mimic the mechanical properties of gastrocnemius lateralis muscle, which has been reported to be around 11 kPa which corresponds to a shear modulus of around 3–4 kPa,[17] and fibrin network of blood clot (0.06–0.6 kPa), respectively.[18] To ensure mechanical coupling of ECs with the gel and to exploit the known benefits of RGD signaling in maintenance of EC function, the CA backbone was functionalized with a peptide presenting the GGGGRGDSP sequence in the N-terminus using aqueous 1-ethyl-3-(3-dimethylaminopropyl)carbodiimide (EDC) chemistry, as previously described.[16] Since RGD ligand density is known to impact cell-biomaterial interaction, the reaction conditions were optimized to ensure the same density of RGD (11.6% ± 0.9% of disaccharide repeat units) in both CA gels.

In order to evaluate the potential angiogenic response of CA hydrogels, four formulations: soft and stiff gels with and without soluble growth factors (GFs) supplementation (GFs: 2.5 ng mL^{-1} of each VEGF, FGF-2, and PMA, i.e., 0.125 ng of each/50 µL of gel injected in the muscle) were implanted into SCID mice gastrocnemius muscles, a target tissue relevant for peripheral artery diseases. The concentration of the growth factors in this cocktail was based on our previous finding that they can promote organization of endothelial cells into lumens in vitro.[16] Hematoxylin and eosin (H&E) staining revealed that after 2 weeks, gels were evident in all conditions and invoked no adverse inflammatory response or foreign-body reaction with no collagenous capsule formation, and thus were well tolerated by the muscle tissue (**Figure 1**a–d). The ability of the CA gels to support the ingrowth of microvessels into its avascular environment was investigated by immunofluorescence and confocal microscopy. All CA gel environments, irrespective of GF supplementation were efficiently invaded by newly formed microvessels, physiologically associated with mural cells, i.e., pericytes (positive for nerve/glial antigen 2 (NG2) and negative for α-smooth muscle actin (α-SMA)), and smooth muscle cells (positive for α-SMA) (Figure 1e–h). The vessel diameters (Figure 1i) were similar in all conditions and the degree of angiogenesis within the gel as measured by the vessel length density (VLD), i.e., the total length of vessels in a given area, was statistically similar between soft and stiff gel formulations regardless of GF supplementation (stiff vs soft and stiff + GF vs soft + GF) (Figure 1j). It is well established that functionality of microvascular networks correlates with branching (short segment length, which depends on the number of branch points in relation to the total amount of vascularity)[19] and a moderate diameter in the range of capillaries (5–10 µm). In this regard, the shortest average segment length interestingly was achieved in the soft gel environment in absence of GF, while in their presence segment length was the highest of all conditions, though not statistically significant (soft = 207.8 ± 48.2 µm, soft + GF = 428.5 ± 103.6 µm, stiff = 277.1 ± 41.3 µm, stiff + GF = 278.5 ± 55.6 µm, $p < 0.01$ soft vs stiff, $p < 0.05$ soft vs stiff + GF, and $p = 0.087$ soft vs soft + GF) (Figure 1k). In order to assess if the capacity of CA gels to support vascular ingrowth could be further improved, CA gels were supplemented with Matrigel (0.01% w/v), a biomaterial known to stimulate angiogenesis due to its optimal combination of basal lamina extracellular matrix and rich content of natural angiogenic growth factors.[20] The choice of the Matrigel concentration was based on our prior studies showing that at this concentration, Matrigel can support EC tubular organization while having no impact on the mechanical properties of the CA gel.[16] After two weeks, we found that Matrigel addition did not affect the integration of the gels in the muscle and did not confer any noticeable benefits over CA gels supplemented with GF and yielded capillary networks that were less branched, as evidenced by longer vascular segments (Figure S1a–g, Supporting Information). Taken together, these data suggest that while both soft and stiff gels were equally effective in inducing initial vascular ingrowth, the addition of growth factors or Matrigel does not confer any significant advantage, but the gel stiffness appears to matter for vessel branching.

To be therapeutically useful, newly induced vascular structures must stabilize, i.e., persist long-term without regression. Since, newly induced vessels require about 4 weeks to become independent of further angiogenic stimuli and persist indefinitely,[8] the fate of initially induced vascular structures (vasculature diameter, length density, and branching) within CA gels with and without GF was characterized 7 weeks after implantation (**Figure 2**a–d). Since GF and Matrigel supplementation yielded similar outcomes, the condition with GF alone was

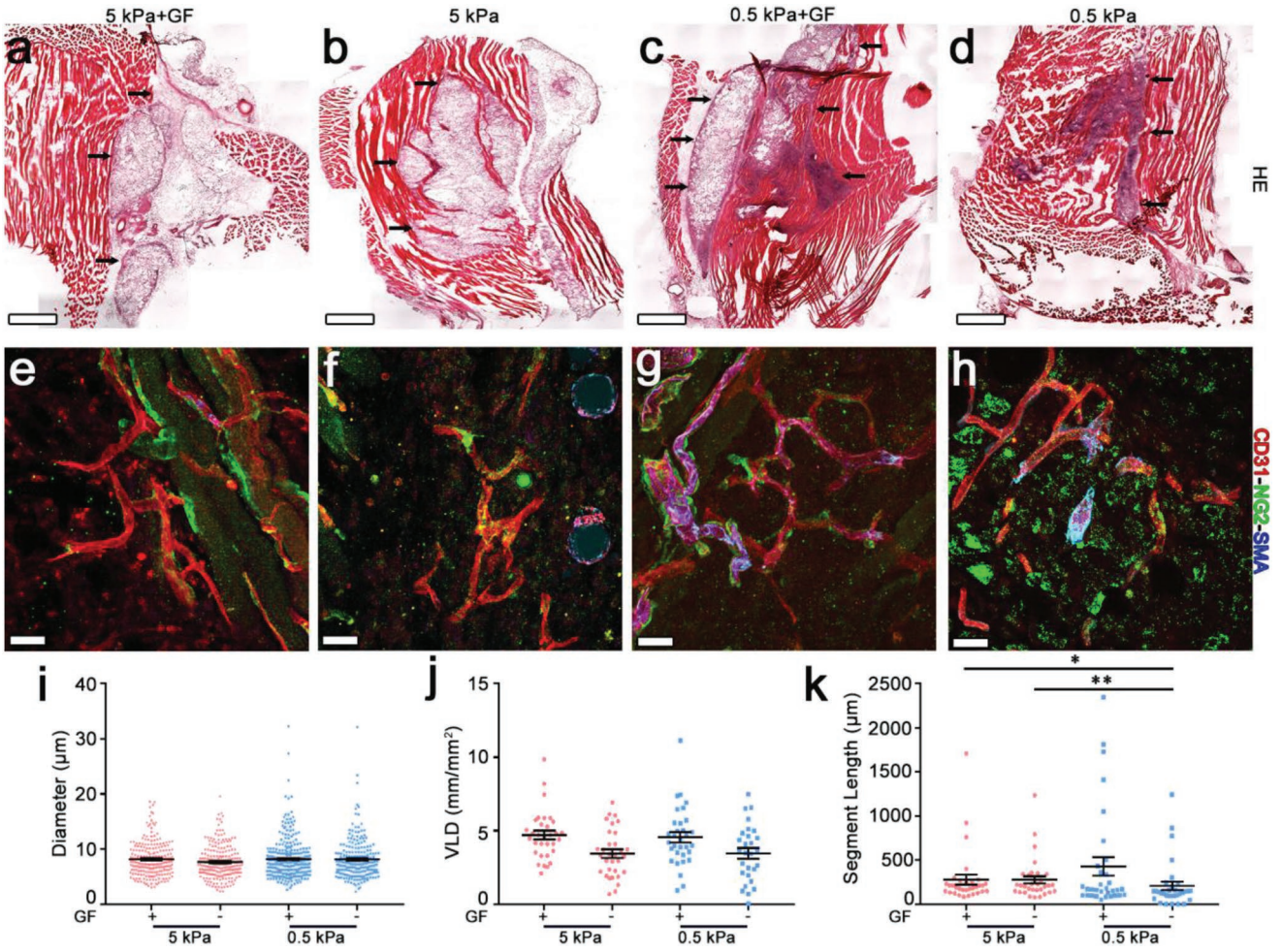

Figure 1. RGD functionalized carboxylated agarose hydrogels induce angiogenesis. a–d) Frozen sections of GC muscles, implanted with distinct hydrogel compositions and harvested after 2 weeks were stained for hematoxylin/eosin and e–h) immunostained against CD31 (endothelial cells, red), NG2 (pericytes, green), α-SMA (smooth muscle cells, cyan). Black arrows in (a–d) indicate the injected gels. Quantification of vessel morphology: i) vessel diameters, j) vessel length density, and k) vascular segment length were quantified in the same areas within the hydrogels two weeks post implantation: VLD = vessel length density, is expressed as millimeters of vessel length per square millimeter of area of effect (mm mm^{-2}). The segment length is expressed as µm of vessel length between two consecutive branch points. GF = growth factors. All data sets represent mean values ± SEM with all individual measurements shown; *$p < 0.05$, **$p < 0.01$ by Kruskal–Wallis test; $n = 4$ independent muscles per each group. Scale bars = 1 mm in all HE-stained panels. Scale bars = 20 µm in all immunofluorescence-stained panels.

included in this experiment in order to account for their role during initial vessel induction.

We made a compelling finding that although vessel diameter was similar among all groups (Figure 2i), vasculature within the stiff gels in the absence of GF showed a significant regression of 50% of VLD when compared to the 2-week time point from 3.4 ± 0.3 to 1.7 ± 0.2 mm mm^{-2} ($p < 0.0001$) (Figure 2j). By contrast, within soft gels similarly deprived of GF not only was the vessel regression arrested, but a further 125% expansion of the vessel network was observed (VLD 2 weeks = 3.6 ± 0.3 mm mm^2, $p < 0.0001$ vs 7 weeks = 8.1 ± 1.3 mm mm^{-2}) resulting in considerably denser vascularity than within the stiffer gels (Figure 2a–h). Further analysis revealed that within the stiff gels vessel regression was accompanied by a reduction in network branching, with a 40% increase in vascular segment length from 277.1 ± 41.3 to 465.2 ± 73.7 µm; whereas within the soft gels capillary networks further increased their branching degree compared to the 2-week time-point regardless of GF supplementation (segment length soft = 117.4 ± 10.5 and soft + GF = 55.3 ± 18.5 µm) (Figure 2k). Once again as in the case at 2 weeks GF supplementation neither increased vessel density within soft gels nor did it promote stabilization (VLD 7 weeks soft + GF = 7.2 ± 1.5 mm mm^{-2} vs soft = 8.1 ± 1.3 mm mm^{-2}, p = n.s.; VLD 2 weeks soft + GF = 5.0 ± 0.8 mm mm^{-2} vs soft = 4.7 ± 0.3 mm mm^{-2}, p = n.s.). Pericytes have been shown to play a crucial role in vessel stabilization, both through secreted and cell contact-dependent signals.[21] While vessels within the stiff gels were scarcely associated with mural cells of any kind (Figure 2a,b and e,f), vessel networks within the soft gels resembled normal muscle capillaries and were associated with NG2$^+$ pericytes (Figure 2c,d), which established tight cell-to-cell contacts with the endothelium (Figure 2g,h). Quantification of pericyte coverage (ratio of vessel length associated with NG2$^+$ pericytes/total vessel length) showed that vascular networks

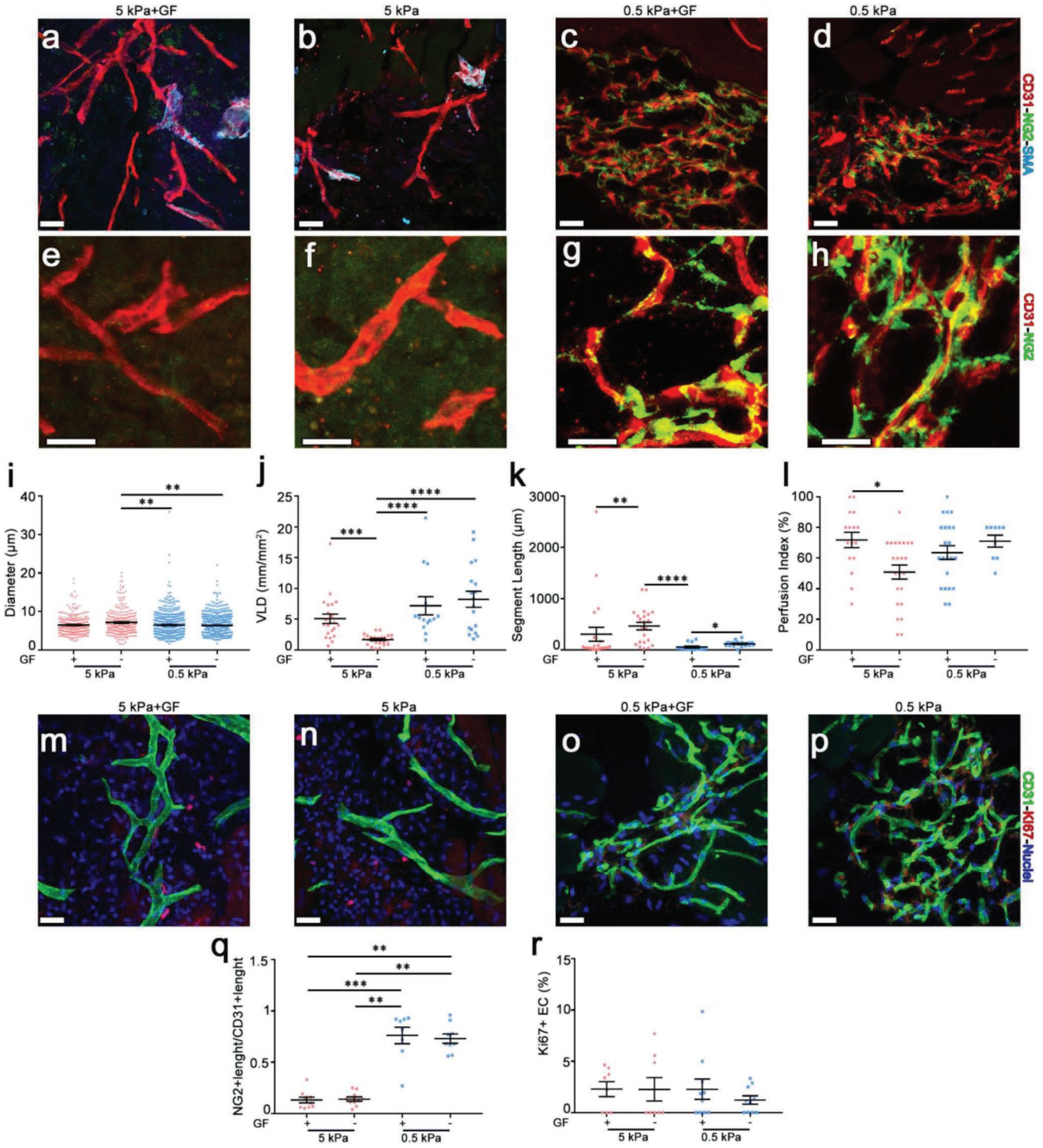

Figure 2. Soft RGD-functionalized carboxylated agarose supports stable capillaries. (a–h) Immunofluorescence staining of endothelium (CD31, in red), pericytes (NG2, in green), smooth muscle cell (α-SMA, in cyan) on frozen sections of leg skeletal muscles of mice injected with distinct hydrogel compositions and sacrificed after 7 weeks. e–h) Higher-magnification panels show the tight association between pericytes and endothelium of vessels in soft gels. i–l) VLD, vascular segment length, vessel diameters, and perfusion index were quantified in the same areas within the hydrogels. GF = growth factors. All data sets represent mean values ± SEM with all individual measurements shown; $^{*}p < 0.05$, $^{**}p < 0.01$, $^{***}p < 0.001$, and $^{****}p < 0.0001$ by Kruskal–Wallis test; $n = 4$ independent muscles per each group. m-p,r) Endothelial proliferation was assessed by quantifying the percentage of endothelial cells positive for Ki67 (r) by immunofluorescence staining on frozen muscle sections (m–p), $n = 4$ independent muscles per group. q) Pericyte coverage was quantified in areas implanted with each hydrogel. Soft gels displayed a marked increase in pericyte coverage compared to stiff gels. Data represent mean values ± SEM; $^{**}p < 0.01$ and $^{***}p < 0.001$ by Kruskal–Wallis test. $n = 4$ independent muscles per each group. Scale bars = 20 µm in all figure panels.

within the soft gels were greater than fivefold more mature compared to those within the stiff gels (soft + GF = 0.76 ± 0.08 vs stiff + GF = 0.13 ± 0.03, $p < 0.001$; and soft = 0.73 ± 0.05 vs stiff = 0.14 ± 0.02, $p < 0.01$; Figure 2q). Considering the large body of work highlighting the challenges associated in controlling complex set of variables (i.e., dose distribution in tissue, duration of stimulation, growth factor splice variants, and their combinations) that impact the induction of physiological angiogenesis by growth factor delivery (either as delivered proteins or by gene therapy),[8,22,23] the ability of a mechanically defined biomaterial environment to induce robust and persistent normal angiogenesis independently of growth factor delivery, as shown here, is particularly attractive.

Newly formed vessels require functional perfusion by the systemic circulation in order to stabilize and persist, as lack of flow in nascent vascular structures, regulated by precapillary arteriole sphincters, is a mechanism by which vascular networks prune redundant vessels and adapt to the metabolic needs of the tissue.[24] Therefore, the establishment of functional blood flow in newly induced vascular structures was assessed by intravenous injection of biotinylated tomato lectin that binds the luminal surface of blood vessels and marks only vessels that are functionally perfused by systemic circulation.[22] Quantification of lectin perfusion showed that vessels in all conditions were well perfused (≈70% of lectin + endothelial structures), with the stiff gels showing a moderate reduction to ≈50% (Figure 2l). This provided evidence that the RGD-modified CA gels support formation of fully functional vascular networks. Since Masson trichrome staining (Figure S2, Supporting Information) revealed that hydrogels persist at the site of implantation even after 7 weeks, induce no foreign-body reaction as assessed by the absence of a collagenous capsule, and support efficient infiltration of host cells, the gels can be considered well integrated in muscle tissue. However, since SCID mice while having a fully functional innate immunity and inflammatory responses, lack B and T lymphocytes, the fate of the gels in immunologically fully competent subjects need to be further assessed in future studies. Taken together, these data suggest that: (a) soft CA gel with mechanical properties similar to fibrin clot specifically promotes new vessel stabilization, yielding long-term persistent and mature (pericyte-associated) microvascular networks with the most optimal functional features of high density and branching complexity, and (b) GF supplementation does not improve the long-term angiogenic effect that are already imposed by the mechanical environment of the gels. Therefore, the observed effects may be attributed to the presence of RGD-modified CA gel environment.

In order to elucidate a biological basis for our observations we explored two scenarios that could promote neovascularization and vessel stabilization namely: (1) differences in proliferation of endothelial cells in the gels, and/or (2) recruiting of circulating support cells. We investigated endothelial proliferation by immunostaining for Ki67, which marks the nucleus of cells in all phases of the cell cycle (G_1, S, G_2, and M), excluding quiescent ones (G_0).[25] Quantification of Ki67$^+$ endothelial nuclei showed that vascular networks in all gel compositions were essentially quiescent after 7 weeks, with at least 98% of ECs in G_0 phase (Figure 2m–p,r). This is consistent with previous findings that in fully normal angiogenesis induced by VEGF 93% of ECs are in the G_0 phase already after 1 week.[26]

It has been shown that circulating myeloid cells can be recruited to sites of active angiogenesis and play a role in both maturation and stabilization of new vessels.[27] In particular, a specific population of CD11b$^+$ monocytes called neuropilin-expressing monocytes, which express Neuropilin-1 (Nrp1), a coreceptor for VEGF and Semaphorin3A coreceptor, has been recently found to accelerate new vessel stabilization by directly activating transforming growth factor-β 1 (TGF-β1) signaling,[22] and indirectly by promoting pericyte recruitment through platelet-derived growth factor-BB (PDGF-BB) secretion.[28] Therefore we investigated whether the long-term stabilization of the capillary networks by the soft gel could relate to a differential enrichment of myeloid cells and specifically promaturative CD11b$^+$ monocytes. Immunofluorescent staining of cryosections of the gels two weeks following implantation revealed that the population of CD45$^+$ myeloid cells was about 40% higher in the softer versus the stiffer gel environment (476.9 ± 37.7 vs 333.8 ± 44.7 cells per field, $p < 0.01$; **Figure 3**a–c), but the enrichment of CD11b$^+$ cells were similar in both gel environments (Figure 3d–f).

Mechanobiology, the paradigm in which mechanical stimuli are translated in biological signals through mechanotransduction elements, has a prominent role in the organization of cells[16] and interaction between cell populations.[29] In addition to signaling via αv integrins, a family of RGD-binding integrins,[30] the stretch-activated ion channel Piezo-1[31]—an integrin activating transmembrane protein, has been shown to have critical role in angiogenesis.[32] Piezo-1 has also been implicated in cell–cell interactions[29] and has been shown to be inherently mechanosensitive.[33] Since the observed differences in the maturation and persistence of vessels are clearly correlated to the vastly differing stiffness of the two gels we inquired if the cells recruited into the gel environment express Piezo-1. Immunofluorescence staining identified for the first time a hitherto unknown population of CD11b$^+$ myeloid cells expressing Piezo-1 (**Figure 4**a,b), which was significantly more frequently found in the softer than in the harder hydrogels, representing 93.1% ± 1.4% of the total CD11b$^+$ cells in the soft gels versus 71.8% ± 2.4% in the stiff gels ($p < 0.0001$; Figure 4c). Since CD11b is also expressed by neutrophils, which can also be recruited to sites of biomaterial implantation up to 2 weeks,[34] we analyzed whether monocytes and/or neutrophils were present in the gels two weeks after implantation by H&E staining by exploiting their easily recognizable and characteristic nuclear morphologies. As shown in Figure S3 of the Supporting Information, both cell types could be identified in gels of both stiffnesses. Based on this finding we further characterized the identity of the CD11b$^+$/Piezo-1$^+$ cells by staining for coexpression of CD11b with the specific markers CD115 for monocytes and Ly6G for neutrophils,[35] and quantified their relative enrichment in the soft versus stiff gels. Interestingly, we identified novel Piezo-1$^+$ subpopulations of both monocytes and neutrophils in both 0.5 and 5 kPa gels (Figure 4d–g). However, quantification of the two populations revealed that only Piezo-1$^+$ monocytes were significantly enriched by about 1.7-fold in soft versus hard gels (0.5 kPa = 40.6% ± 4.6% of total

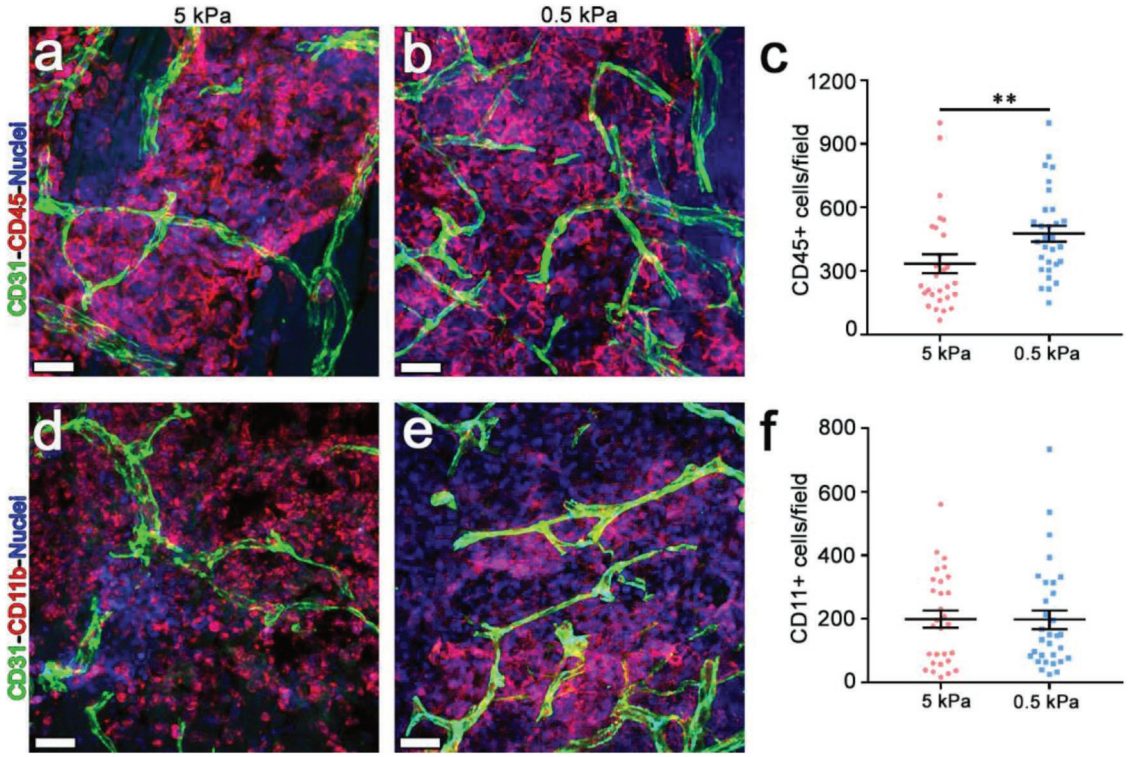

Figure 3. RGD functionalized carboxylated agarose recruit myeloid cells. a,b,d,e) Immunofluorescence staining of endothelial cells (CD31, in green), leukocyte (CD45, in red) and monocytes (CD11b, in red) on cryosections of limb muscles 2 week after injection with 5 and 0.5 kPa hydrogel compositions. Scale bar = 20 µm in all panels. c,f) Quantification of the number of $CD45^+$ and $CD11b^+$ cells recruited into the implanted hydrogel. All data sets represent mean values ± SEM with all individual measurements shown; $^{**}p < 0.01$, by Mann–Whitney test; $n = 4$ independent muscles per each group.

$CD11b^+$ cells vs 5 kPa = 24.4% ± 2.6%, $p < 0.01$; Figure 4h), whereas Piezo-1^+ neutrophils were similarly frequent in the two conditions (0.5 kPa = 25.4% ± 3.9% vs 5 kPa = 19.5% ± 2.0%, p = n.s.; Figure 4h).

In order to ascertain if Piezo-1^+ myeloid populations exist in the circulation and are enriched into the gels, or if Piezo-1 expression is induced upon exposure to the gel microenvironment, both mouse and human peripheral blood mononuclear cells were analyzed using flow cytometry. Human cells were also analyzed in order to establish the validity of the results in a translational perspective. A population of Piezo-1-expressing $CD11b^+$ cells was identified in the circulation of both mouse and healthy human donors (Figure 4i,j), with surprisingly similar frequency, accounting for 35.0% ± 2.2% and 35.1% ± 9.1% of total $CD11b^+$ cells, respectively. However, further separation of the $CD11b^+$ population between monocytes and neutrophils, based on mutually exclusive expression of CD115 and Ly6G (mouse) or CD14 and CD66b (human), showed that a Piezo-1^+ subpopulation could be found only in circulating monocytes, but not in neutrophils (Figure 4k,l), with similar frequency in both mouse and human blood (46.9% ± 18.5% and 48.5% ± 15.9% of total monocytes, respectively; Figure 4m,n).

Therefore, these data suggest that a population of mechanosensitive $CD11b^+/CD115^+/Piezo1^+$ monocytes exist in normal circulation and that they can accumulate in CA hydrogels in differential manner based on their mechanical properties. The basis for this enrichment of $CD11b^+$/Piezo-1^+ population within CA gels could be either due to increased survival or retention or both and needs further investigation. On the other hand, mechanosensitive neutrophils could not be found in the circulation, but were observed in the CA gels, suggesting the possibility that Piezo-1 expression in this case may be mainly induced by the gel environment. The role of immune cells in regenerative medicine is an emerging theme. It has been recently shown that T helper 2 (Th2) lymphocytes, which comprise adaptive immunity play an important role in facilitating muscle tissue regeneration by ECM-based biomaterials.[36] Interestingly, our data show that the purely angiogenic effect of vessel stabilization by a mechanically defined environment does not require adaptive immunity, as this is lacking in the SCID mice. It is worth noting that in pulmonary inflammation recruitment of $CD11b^+$ myeloid cells have been found to be critical in the homing of activated Th2 lymphocytes and orchestration of an adaptive immune response.[37] Since the introduction of the gel in the muscle environment is bound to invoke an inflammatory response, the presence of $CD11b^+$ cells could be a consequence of an inflammatory response. Considering these observations and the recently identified functions of $CD11b^+$ monocytes in regulating the stabilization of newly induced vessels,[22] the novel population of $CD11b^+/CD115^+/Piezo1^+$ monocytes identified here may represent the link between the mechanics and angiogenic properties of hydrogels and represents a novel direction for future efforts in developing systems and pharmacological agents for therapeutic angiogenesis.

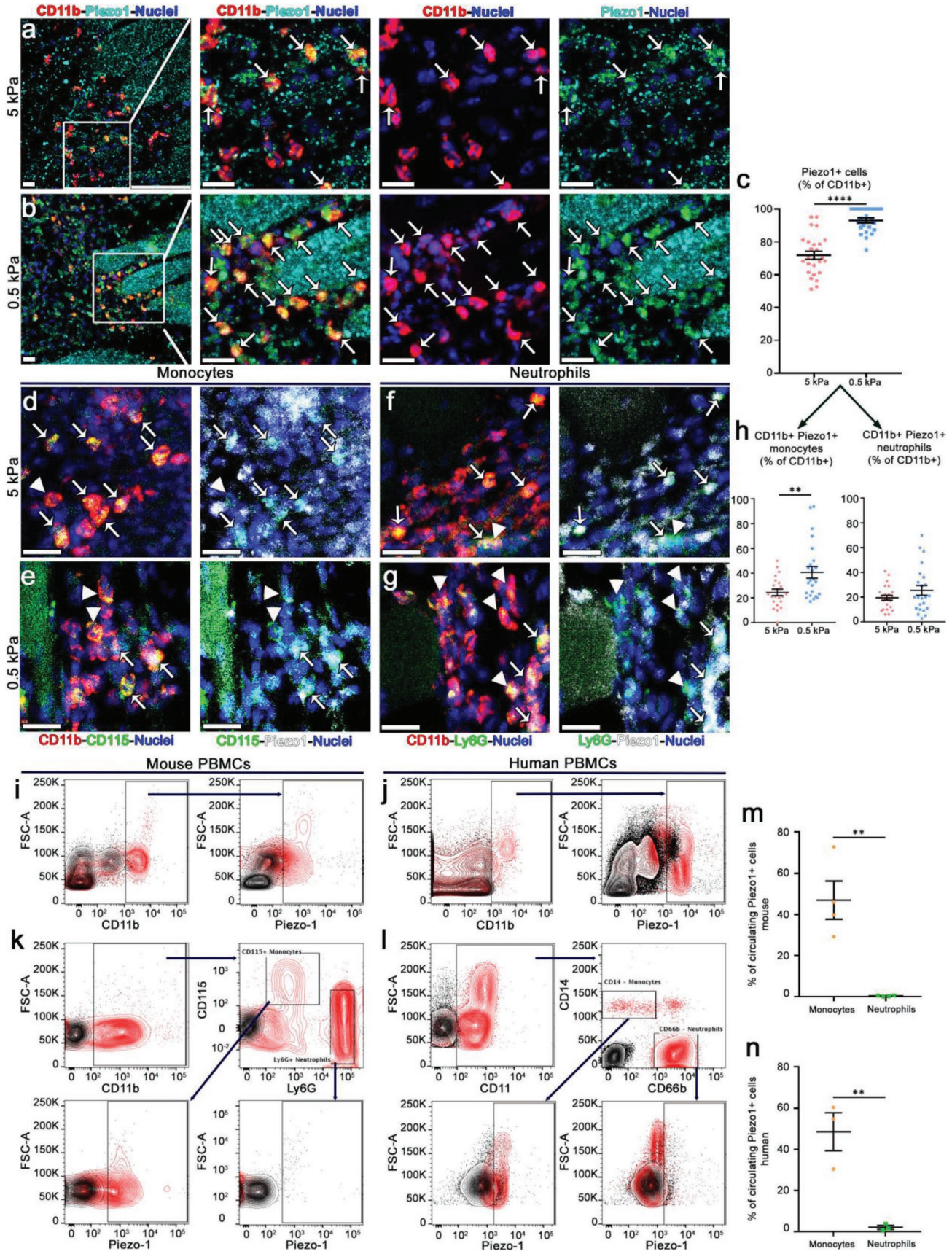

Experimental Section

Gels Preparation and Characterization: Native agarose (1 g) (Merck, Darmstadt, Germany) was transferred into a 3-necked round-bottom flask equipped with a mechanical stirrer and pH-meter (WTW, Weinheim, Germany), and dissolved in deionized water at a concentration of 1% w/v by heating to 90 °C. The flask was cooled down to 0 °C, using an ice bath, under vigorous mechanical stirring in order to prevent gelation of the agarose, and the reactor was charged with 99% (2,2,6,6-tetramethylpiperidin-1-yl)oxyl (20.6 mg, 0.16 mmol), NaBr (0.1 g, 0.9 mmol), and NaOCl (2.5 mL, 15% solution) all obtained from Sigma-Aldrich (Steinheim, Germany). As the reaction proceeds, the solution becomes acidic. The pH of the solution was maintained at 10.8 by dropwise addition of NaOH (0.1 M) (Sigma-Aldrich, Steinheim, Germany) throughout the duration of the reaction. The degree of carboxylation was back calculated by using the volumes of NaOH (0.1 M) solution added during the reaction. The reaction was quenched by the addition of $NaBH_4$ (0.1 g) (Sigma-Aldrich, Steinheim, Germany), following which the solution was acidified to pH 8 (0.1 mHCl) and stirred for 1 h. The modified agarose was then precipitated by the sequential addition of NaCl (12 g, 0.2 mol) and ethanol (500 mL) (technical grade). The product was collected by vacuum filtration using a fritted glass funnel and then washed using ethanol (500 mL). The ethanol, catalyst, and salts were removed by extensive dialysis against water for 2 days with replacement of the water every 12 h. The modified agarose was then freeze-dried on a Beta 2–8 LD (Martin Christ Gefriertrocknungsanlagen GmbH, Osterode am Harz, Germany) overnight to yield a white solid. The degree of carboxylation was verified by the appearance of peaks associated with aliphatic carboxylic acid groups via FTIR (KBr) (νc = o: 1750 cm^{-1}) (Bruker Optics, Ettlingen, Germany) and NMR 300 Mhz (^{13}C: 180 ppm) (Bruker BioSpin, Rheinstetten, Germany). The number average molecular weight of CA was determined as described earlier[16] and was in the range of 83 000–95 000.

Carboxylated Agarose Mechanical Properties: Rheology experiments were performed with a Physica MCR 301 (Anton Paar, Wundschuh, Austria) equipped with a Peltier cell to control the temperature and the experiment was performed with a plate geometry PPR25 (Anton Paar, Wundschuh, Austria). Samples in deionized water were prepared by heating at 90 °C for 10 min until a clear solution was obtained. The liquid was then poured on the rheometer plate and the following sequence was used to determine the shear modulus: cool down from 80 to 5 °C in 30 min, 30 min equilibration at 5 °C to allow the gel to form, followed by heating to 37 °C and equilibration for 30 min prior to measuring G′ and G″ by increasing the rotation frequency from 0.01 up to 10 rad s^{-1} with a 1% deformation. The G′ of the gel was determined at 1 Hz shear frequency.

Carboxylated Agarose RGD Functionalization: Functionalization of CA with the RGDSP (Peptides International, Louisville, Kentucky, USA) peptide was performed using EDC (Sigma-Aldrich Chemie GmbH, Steinheim, Germany) coupling chemistry. CA was sterilized overnight in 70% ethanol, and the ethanol was removed by extensive dialysis against water. The sterile CA was freeze-dried overnight to yield a white solid. CA (30 mg, 0.25 µmol) was dissolved in MES sterile buffer (Sigma-Aldrich Chemie GmbH, Steinheim, Germany) and an excess EDC (210 mg, 1.3 mmol) was added and the solution stirred for 30 min. Following this the peptide was added (500 µg, 0.66 µmol for the CA-60 gels and 1 mg, 1.33 µmol for the gels) and the solution stirred for an additional 2 h at room temperature. Unreacted reagents were removed by dialysis against water. RGD incorporation was verified using elemental analysis Vario EL (Elementar Analysen systeme GmbH, Langenselbold, Germany) equipped with a thermal conductivity detector and an adsorption column for CO_2 at 110 °C and H_2O at 150 °C. All samples were accurately weighed to 3 mg before measurements and the percentage of nitrogen was used to calculate the peptide attachment. It was found that 11.6% ± 0.9% of the repeat units where functionalized on both CA-28 and CA-60.

Gels Implantation In Vivo: Gels were implanted into 10–15 week old immune-deficient SCID CB.17 mice (Charles River Laboratories, Sulzfeld, Germany). Gels were pre-loaded in 1 mL syringes and kept on ice (≈4 °C) until injection. 50 µL of cold PBS (Sigma-Aldrich Chemie GmbH, Steinheim, Germany) followed by 50 µL of cooled gels were implanted along the midline of both the medialis and lateralis portions of Gastrocnemius leg muscle in a standard caudo-rostral direction, using a syringe with a $29^1/_2$G needle (Becton Dickinson, Allschwil, Switzerland). Gels supplemented with growth factors were loaded with 50 ng mL^{-1} of each VEGF, FGF-2 both from R&D Systems (Minneapolis, USA), and PMA from Sigma-Aldrich (Munich, Germany).

Tissue Staining and Microscopy: For the studies performed on frozen tissue sections, mice were anesthetized and the tissues were fixed by vascular perfusion of 1% paraformaldehyde in PBS pH 7.4 for 4 min under 120 mm Hg^{-1} of pressure. GC muscles were harvested, post fixed in 0.5% paraformaldehyde in PBS for 2 h, cryoprotected in 30% sucrose in PBS overnight at 4 °C, embedded in OCT compound (CellPath, Newtown, Powys, UK), frozen in freezing isopentane and cryosectioned. Cryosections were obtained systematically in a caudo-rostral direction throughout the whole sample, maintaining an anatomically standardized orientation, and analyses were performed on all sections representing the complete area of implantation. Tissue sections (30 µm) were stained with H&E and in addition, the gel biocompatibility was examined with Masson trichrome staining (Réactifs RAL, Martillac, France), performed according to manufacturer's instructions. For immunofluorescent staining of neighboring 30 µm thick longitudinal cryosections, the sections were blocked with PBS 0.1% triton supplemented with 5% normal goat or donkey serum and 2% BSA (all reagents from Sigma-Aldrich Chemie GmbH, Steinheim, Germany) for 1 h. The slides were then incubated for 1.5 h at room temperature with the following primary antibodies and dilutions: rat anti-mouse PECAM-1 (clone MEC 13.3, BD Biosciences, Basel, Switzerland) at 1:100 or hamster monoclonal anti-mouse CD31 (clone 2H8, Millipore, Merck, Germany) at 1:200; mouse anti-mouse/human α-SMA (clone 1A4, MP Biomedicals, Basel, Switzerland) at 1:400; anti-mouse NG2 (Chemicon International, Hampshire, UK) at 1:200; rabbit anti-Ki67 (Abcam, Cambridge, UK) at 1:100; rat monoclonal anti-CD11b (clone M1/70, Abcam, Cambridge, UK) at 1:100; rat anti-mouse CD45 (PE conjugated, clone 30 F11, BD Biosciences, Basel, Switzerland) at 1:400. Negative controls lacking primary antibody were always performed. Sections were rinsed in

Figure 4. $CD11b^+/CD115^+/Piezo\text{-}1^+$ monocytes are enriched in soft RGD-functionalized carboxylated agarose microenvironment. a,b) Immunofluorescence staining of $CD11b^+$ cells (in red) and of $PIEZO\text{-}1^+$ cells (in light blue) on cryosections of limb muscles 2 weeks after injection with 5 and 0.5 kPa hydrogel compositions. Scale bar = 20 µm in all panels. c) Quantification of $CD11b^+/Piezo1^+$ cells in sites within the implanted gels (% of total $CD11b^+$ cells). d–g) Immunofluorescence staining of CD11b (in red), CD115 (in green), Ly6G (in green), and PIEZO-1 (in white) on cryosections of limb muscles. White arrows and arrowheads in panels (d) and (e) indicate $Piezo\text{-}1^+$ and $Piezo\text{-}1^-$ monocytes ($CD11b^+/CD115^+$), respectively. White arrows and arrowheads in panels (f) and (g) similarly indicate $Piezo\text{-}1^+$ and $Piezo\text{-}1^-$ neutrophils ($CD11b^+/Ly6G^+$), respectively. Scale bar = 20 µm in all panels. h) Quantification of $Piezo1^+$ monocytes and $Piezo1^+$ neutrophils in sites within the implanted gels (% of total $CD11b^+$ cells). i,j) Circulating $Piezo\text{-}1^+/CD11b^+$ cells were identified in both mouse and human blood by FACS. k) Detection of circulating $Piezo\text{-}1^+$ monocytes ($CD11b^+/CD115^+/Ly6G^-$) and neutrophils ($CD11b^+/CD115^-/Ly6G^+$) in mouse blood. l) Detection of circulating $Piezo\text{-}1^+$ monocytes ($CD11b^+/CD14^+/CD66b^-$) and neutrophils ($CD11b^+/CD14^-/CD66b^+$) in human blood. m,n) Quantification of circulating $Piezo\text{-}1^+$ monocytes and $Piezo\text{-}1^+$ neutrophils in mouse and human blood respectively (% of total monocytes or neutrophils). All data sets represent mean values ± SEM with all individual measurements shown; $^{****}p < 0.0001$ and $^{**}p < 0.01$ by unpaired *t*-test (c) or by Mann–Whitney test (h,m,n). FACS experiment: $n = 4$ mice and $n = 3$ human donors.

PBS 0.1% triton and then incubated for 1.5 h at room temperature with fluorescently labeled secondary antibodies (Invitrogen, Basel, Switzerland) diluted at 1:200. The slides were then rinsed and mounted.

Piezo1 staining immunohistochemistry experiments were performed on Ventana DiscoveryUltra instrument (Roche Diagnostics, Mannheim, Germany) by using the procedure RUO Discovery Universal instead. Cryosections were fixed for 12 min with 4% paraformaldehyde followed by 1 h incubation at 37 °C with rat anti-CD11b (1:100), alone or together with rat monoclonal anti-CD115 (clone CSF-1R, Biolegend, London, UK) at 1:100 or rat monoclonal anti-Ly6G (clone 1A8, Biolegend, London, UK) at 1:100, and 32 min incubation at 37 °C with fluorescently labeled anti-rat IgG1 or IgG2a secondary antibodies used at 1:100 (ThermoFisher Scientific, Basel, Switzerland). Next, after an antibody denaturation step, sections were pretreated for 16 min with cell conditioning solution (CC1) (Roche Diagnostics, Mannheim). Rabbit anti-Piezo1 (Proteintech, Manchester, UK) diluted at 1:500 was then incubated for 32 min at 37 °C and detected with the secondary antibody (ImmPRESS reagent kit peroxidase anti-rabbit Ig MP-7401, Vector Laboratories, Burlingame, CA, USA) applied manually (200 µL) for 32 min. Discovery Rhodamine (Roche Diagnostics, Mannheim) applied for 12 min was used for the detection. To study vessel perfusion, 100 µg of biotinylated Lycopersicon esculentum (tomato) lectin (Vector Laboratories, Burlingame, CA, USA) was dissolved in 100 µL, which binds the luminal surface of all blood vessels, and injected intravenously through the femoral vein. After 4 min the thoracic cavity was opened and the tissues were fixed by perfusing the animal with 1% paraldehyde and leg muscle were collected and processed as described above. Fluorescently labeled Streptavidin (eBioscience, Vienna, Austria) at 1:200 was used to visualize the perfused vasculature. Frozen sections were mounted with Faramount Aqueous Mounting Medium (Dako, Agilent Technologies, Basel, Switzerland), and fluorescence images were taken with 40× objectives on a Carl Zeiss LSM710 3-laser scanning confocal microscope (Carl Zeiss, Feldbach, Switzerland) or with a 20× objective on an Olympus B×61 microscope (Olympus, Volketswil, Switzerland). All Image analysis were performed with either Cell Sense software (Olympus, Volketswil, Switzerland) or Imaris 7.6.5 software (Bitplane, Zürich, Switzerland) on fluorescence images acquired with a 20× objective on an Olympus BX61 microscope or with a 40× objective on a Carl Zeiss LSM710 3-laser scanning confocal microscope.

Histological Analysis: The quantification of VLD and vessel perfusion was performed on sections of leg muscles harvested after intravascular staining with biotinylated lectin and fluorescently labeled streptavidin, as described above. After costaining with a fluorescent anti-CD31 antibody, VLD was measured on 6–10 randomly acquired fields per leg and 4 muscles per group ($n = 4$) by tracing the total length of vessels in the fields and dividing it by the area of the fields. The total lengths of lectin-positive and CD31-positive vascular structures in each field were traced independently and the vessel perfusion index was calculated as the ratio between the two values. The degree of branching of a vascular network depends on the total number of branch points in relation to the total amount of vascularity. Therefore, the degree of vessel branching was quantified by counting the number of branch points (n) in all representative fields per muscles and dividing the corresponding total vessel length by $n + 1$, yielding the average vascular segment length. Vessel diameters were measured by overlaying a captured microscopic image with a square grid. Squares were chosen at random, and the diameter of each vessel (if any) in the center of selected squares was measured. 2 to 5OO total vessel diameter measurements were obtained from 4 muscles per each group ($n = 4$). The quantification of pericyte coverage was performed on sections of leg muscles after immunostaining for endothelium (CD31) and pericytes (NG2). The total lengths of CD31- and NG2-positive structures were measured by a blinded investigator and the pericyte coverage index was calculated as the ratio between the two values. $Ki67^+$ ECs were quantified from the total number of ECs (260-890 total ECs were counted per condition at 7 weeks post gel implantation) in vascular structures visible in each of 3–5 fields, in each area of effect. Ten areas with a clear angiogenic effect were analyzed per group. The quantification of leukocytes (CD45) and monocyte (CD11b) were performed on seven random areas per muscle ($n = 4$) per group by counting them and normalizing to the absolute number of $CD45^+$ and $CD11b^+$ cells with area. (9000–1400 total $CD45^+$ cells and 5000–6000 total $CD11^+$ cells were counted per condition at 2 weeks post gel implantation). The quantification of $Piezo1^+/CD11b^+$ cells was performed on 7–10 random areas per muscle ($n = 4$ samples per group) after immunostaining for CD11b (700–800 total $CD11^+$ cells were counted per condition at 2 weeks post gel implantation). The quantification of $Piezo1^+/CD11b^+/$ $CD115^+$ monocytes and $Piezo1^+/CD11b^+/Ly6G^+$ neutrophils was performed on 5–7 random areas per muscle ($n = 4$ samples per group) after immunostaining for CD11b, CD115 or Ly6G (480–900 total $CD11b^+$ cells were counted per condition at 2 weeks post gel implantation).

All image measurements were performed with both Cell Sense software (Olympus, Volketswil, Switzerland) and Imaris 7.6.5 software on fluorescence images acquired with a 20× objective on an Olympus BX61 microscope or with a 40× objective on a Carl Zeiss LSM710 3-laser scanning confocal microscope.

Blood Cell Analysis by FACS: Peripheral blood mononuclear cells (PBMCs) were isolated from the whole blood of four immune-deficient SCID CB.17 mice (Charles River Laboratories, Sulzfeld, Germany) and three human healthy donors using a red blood cell lysis buffer (RBC Lysis Buffer, Invitrogen, Basel, Switzerland). After lysis, the PBMCs were stained with APC-anti-human CD11b (clone CBRM1/5, Biolegend, Basel, Switzerland) at 1:100, PE-anti-human CD66b (clone G10F5, Biolegend, Basel, Switzerland) at 1:100 and BV711-anti-human CD14 (clone M5E2, Biolegend, Basel, Switzerland) at 1:100, or BV605-anti-mouse-CD11b (clone M1/70, Biolegend, Basel, Switzerland) at 1:100, PE-anti-mouse-Ly6G (clone 1A8, BD Biosciences, Basel, Switzerland) at 1:100, APC-anti-mouse-CD115 (clone AFS98, BD Biosciences, Basel, Switzerland) at 1:100. A cross-reacting anti-human Piezo1 (Abcam, Cambridge, UK) was used at 1:500 for both human and mouse cells. An Alexa Fluor 488-labeled secondary antibody was used to detect Piezo1 (Invitrogen, Basel, Switzerland) at 1:200. Samples were acquired by LSR Fortessa (BD Biosciences, Basel, Switzerland), and data analyzed by FlowJo software (Tree Star, Ashland, OR, USA).

Statistical Analysis: Data are presented as mean ± standard error. All quantifications have been performed by blinded investigators to avoid bias. The significance of differences was assessed with the GraphPad Prism 7.03 software (GraphPad Software). The normal distribution of all data sets was tested and, depending on the results, multiple comparisons were performed with the parametric 1-way analysis of variance (ANOVA) followed by the Sidak test for multiple comparisons, or with the nonparametric Kruskal–Wallis test followed by Dunn's post-test, while single comparisons were analyzed with the nonparametric Mann–Whitney test or the parametric unpaired t-test.

Ethical Statement: Animals were treated in accordance with Swiss Federal guidelines for animal welfare, and the study protocol was approved by the Veterinary Office of the Canton of Basel-Stadt (Basel, Switzerland; Permit 2071). Human blood cells were obtained from healthy volunteers following informed consent.

Supporting Information

Supporting Information is available from the Wiley Online Library or from the author.

Acknowledgements

A.F., R.G.-B., A.B., and V.P.S. contributed equally to this work. This work was funded by the excellence initiative of the German Federal and State Governments Grant EXC 294 and Swiss National Foundation grant (163202 to A.B.) V.P.S. and A.F. conceived the study. A.F., R.G.B., A.B., and V.P.S. designed the study. A.F., R.G.B., A.U., M.S., E.K., B.F., M.G.M., and S.B. carried out experiments, A.F., R.G.B., A.U., M.S., K.A., A.B., and V.P.S. analyzed data, and A.F., R.G.B., M.S., A.B., and V.P.S. wrote the manuscript.

Conflict of Interest

A.B., A.F., R.G.-B., and V.P.S. are named as inventors in patent applications.

Keywords

carboxylated agarose, mechanobiology, Piezo-1, therapeutic angiogenesis, vessel stabilization

Received: December 13, 2018
Published online:

[1] S. Takeshita, L. P. Zheng, E. Brogi, M. Kearney, L. Q. Pu, S. Bunting, N. Ferrara, J. F. Symes, J. M. Isner, *J. Clin. Invest.* **1994**, *93*, 662.
[2] a) J. K. Leach, D. Kaigler, Z. Wang, P. H. Krebsbach, D. J. Mooney, *Biomaterials* **2006**, *27*, 3249; b) E. A. Silva, D. J. Mooney, *J. Thromb. Haemostasis* **2007**, *5*, 590.
[3] a) F. W. Sellke, R. J. Laham, E. R. Edelman, J. D. Pearlman, M. Simons, *Ann. Thoracic Surge.* **1998**, *65*, 1540; b) H. Hosseinkhani, M. Hosseinkhani, A. Khademhosseini, H. Kobayashi, Y. Tabata, *Biomaterials* **2006**, *27*, 5836; c) H. H. Chu, J. Gao, C. W. Chen, J. Huard, Y. D. Wang, *Proc. Natl. Acad. Sci. USA* **2011**, *108*, 13444.
[4] a) T. Asahara, T. Murohara, A. Sullivan, M. Silver, R. van der Zee, T. Li, B. Witzenbichler, G. Schatteman, J. M. Isner, *Science* **1997**, *275*, 964; b) S. Kaushal, G. E. Amiel, K. J. Guleserian, O. M. Shapira, T. Perry, F. W. Sutherland, E. Rabkin, A. M. Moran, F. J. Schoen, A. Atala, S. Soker, J. Bischoff, J. E. Mayer, *Nat. Med.* **2001**, *7*, 1035.
[5] a) M. L. Springer, G. Hortelano, D. M. Bouley, J. Wong, P. E. Kraft, H. M. Blau, *J. Gene Med.* **2000**, *2*, 279; b) A. Banfi, G. von Degenfeld, R. Gianni-Barrera, S. Reginato, M. J. Merchant, D. M. McDonald, H. M. Blau, *FASEB J.* **2012**, *26*, 2486.
[6] a) J. M. Isner, K. Walsh, J. Symes, A. Pieczek, S. Takeshita, J. Lowry, S. Rossow, K. Rosenfield, L. Weir, E. Brogi, R. Schainfeld, *Circulation* **1995**, *91*, 2687; b) D. W. Losordo, P. R. Vale, J. F. Symes, C. H. Dunnington, D. D. Esakof, M. Maysky, A. B. Ashare, K. Lathi, J. M. Isner, *Circulation* **1998**, *98*, 2800; c) T. T. Rissanen, I. Vajanto, S. Yla-Herttuala, *Eur. J. Clin. Invest.* **2001**, *31*, 651; d) M. Giacca, S. Zacchigna, *Gene Ther.* **2012**, *19*, 622.
[7] a) M. Kubo, T. S. Li, R. Suzuki, B. Shirasawa, N. Morikage, M. Ohshima, S. L. Qin, K. Hamano, *Am. J. Physiol.: Heart Circ. Physiol.* **2008**, *294*, H590; b) T. S. Li, K. Hamano, K. Suzuki, H. Ito, N. Zempo, M. Matsuzaki, *Am. J. Physiol.: Heart Circ. Physiol.* **2002**, *283*, H468; c) M. Kubo, T. S. Li, H. Kurazumi, Y. Takemoto, M. Ohshima, K. Hamano, *Circulation* **2018**, *124*, A9198.
[8] C. R. Ozawa, A. Banfi, N. L. Glazer, G. Thurston, M. L. Springer, P. E. Kraft, D. M. McDonald, H. M. Blau, *J. Clin. Invest.* **2004**, *113*, 516.
[9] G. Bergers, S. Song, *Neuro-Oncology* **2005**, *7*, 452.
[10] a) M. Murakami, *Int. J. Vasc. Med.* **2012**, *2012*, 293641; b) M. S. Wietecha, W. L. Cerny, L. A. DiPietro, *Curr. Top. Microbiol.* **2013**, *367*, 3.
[11] a) N. Koike, D. Fukumura, O. Gralla, P. Au, J. S. Schechner, R. K. Jain, *Nature* **2004**, *428*, 138; b) P. Au, J. Tam, D. Fukumura, R. K. Jain, *Blood* **2008**, *111*, 4551.
[12] A. C. Newman, M. N. Nakatsu, W. Chou, P. D. Gershon, C. C. W. Hughes, *Mol. Biol. Cell* **2011**, *22*, 3791.
[13] C. J. Avraamides, B. Garmy-Susini, J. A. Varner, *Nat. Rev. Cancer* **2008**, *8*, 604.
[14] S. H. Kim, J. Turnbull, S. Guimond, *J. Endocrinol.* **2011**, *209*, 139.
[15] D. E. Ingber, *Proc. Natl. Acad. Sci. USA* **1990**, *87*, 3579.
[16] A. Forget, J. Christensen, S. Ludeke, E. Kohler, S. Tobias, M. Matloubi, R. Thomann, V. P. Shastri, *Proc. Natl. Acad. Sci. USA* **2013**, *110*, 12887.
[17] a) E. J. Chen, J. Novakofski, W. K. Jenkins, W. D. OBrien, *IEEE Trans. Sonics Ultrason.* **1996**, *43*, 191; b) K. Lima, J. F. S. Costa Junior, W. C. A. Pereira, L. F. Oliveira, *Ultrasonography* **2018**, *37*, 3.
[18] M. D. Bale, M. F. Muller, J. D. Ferry, *Biopolymers* **1985**, *24*, 461.
[19] A. J. LeBlanc, L. Krishnan, C. J. Sullivan, S. K. Williams, J. B. Hoying, *Microcirculation* **2012**, *19*, 676.
[20] a) M. L. Ponce, *Methods Mol. Biol.* **2009**, *467*, 183; b) K. M. Malinda, *Methods Mol. Biol.* **2009**, *467*, 287.
[21] K. Gaengel, G. Genove, A. Armulik, C. Betsholtz, *Arterioscler., Thromb., Vasc. Biol.* **2009**, *29*, 630.
[22] E. Groppa, S. Brkic, E. Bovo, S. Reginato, V. Sacchi, N. Di Maggio, M. G. Muraro, D. Calabrese, M. Heberer, R. Gianni-Barrera, A. Banfi, *EMBO Mol. Med.* **2015**, *7*, 1366.
[23] W. W. Yuen, N. R. Du, C. H. Chan, E. A. Silva, D. J. Mooney, *Proc. Natl. Acad. Sci. USA* **2010**, *107*, 17933.
[24] M. Potente, H. Gerhardt, P. Carmeliet, *Cell* **2011**, *146*, 873.
[25] T. Scholzen, J. Gerdes, *J. Cell. Physiol.* **2000**, *182*, 311.
[26] R. Gianni-Barrera, M. Trani, C. Fontanellaz, M. Heberer, V. Djonov, R. Hlushchuk, A. Banfi, *Angiogenesis* **2013**, *16*, 123.
[27] C. Murdoch, M. Muthana, S. B. Coffelt, C. E. Lewis, *Nat. Rev. Cancer* **2008**, *8*, 618.
[28] S. Zacchigna, L. Pattarini, L. Zentilin, S. Moimas, A. Carrer, M. Sinigaglia, N. Arsic, S. Tafuro, G. Sinagra, M. Giacca, *J. Clin. Invest.* **2008**, *118*, 2062.
[29] N. R. Blumenthal, O. Hermanson, B. Heimrich, V. P. Shastri, *Proc. Natl. Acad. Sci. USA* **2014**, *111*, 16124.
[30] S. M. Weis, D. A. Cheresh, *Cold Spring Harbor Perspect. Med.* **2011**, *1*, a006478.
[31] B. Nilius, *EMBO Rep.* **2010**, *11*, 902.
[32] a) J. Li, B. Hou, S. Tumova, K. Muraki, A. Bruns, M. J. Ludlow, A. Sedo, A. J. Hyman, L. McKeown, R. S. Young, N. Y. Yuldasheva, Y. Majeed, L. A. Wilson, B. Rode, M. A. Bailey, H. R. Kim, Z. Fu, D. A. Carter, J. Bilton, H. Imrie, P. Ajuh, T. N. Dear, R. M. Cubbon, M. T. Kearney, R. K. Prasad, P. C. Evans, J. F. Ainscough, D. J. Beech, *Nature* **2014**, *515*, 279; b) S. S. Ranade, Z. Z. Qiu, S. H. Woo, S. S. Hur, S. E. Murthy, S. M. Cahalan, J. Xu, J. Mathur, M. Bandell, B. Coste, Y. S. J. Li, S. Chien, A. Patapoutian, *Proc. Natl. Acad. Sci. USA* **2014**, *111*, 10347.
[33] R. Syeda, M. N. Florendo, C. D. Cox, J. M. Kefauver, J. S. Santos, B. Martinac, A. Patapoutian, *Cell Rep.* **2016**, *17*, 1739.
[34] S. Jhunjhunwala, S. Aresta-DaSilva, K. Tang, D. Alvarez, M. J. Webber, B. C. Tang, D. M. Lavin, O. Veiseh, J. C. Doloff, S. Bose, A. Vegas, M. Ma, G. Sahay, A. Chiu, A. Bader, E. Langan, S. Siebert, J. Li, D. L. Greiner, P. E. Newburger, U. H. von Andrian, R. Langer, D. G. Anderson, *PLoS One* **2015**, *10*, e0137550.
[35] B. N. Jaeger, J. Donadieu, C. Cognet, C. Bernat, D. Ordonez-Rueda, V. Barlogis, N. Mahlaoui, A. Fenis, E. Narni-Mancinelli, B. Beaupain, C. Bellanne-Chantelot, M. Bajenoff, B. Malissen, M. Malissen, E. Vivier, S. Ugolini, *J. Exp. Med.* **2012**, *209*, 565.
[36] K. Sadtler, K. Estrellas, B. W. Allen, M. T. Wolf, H. Fan, A. J. Tam, C. H. Patel, B. S. Luber, H. Wang, K. R. Wagner, J. D. Powell, F. Housseau, D. M. Pardoll, J. H. Elisseeff, *Science* **2016**, *352*, 366.
[37] B. D. Medoff, E. Seung, S. Hong, S. Y. Thomas, B. P. Sandall, J. S. Duffield, D. A. Kuperman, D. J. Erle, A. D. Luster, *J. Immunol.* **2009**, *182*, 623.